analytical chemistry

Article

Cite This: *Anal. Chem.* 2019, 91, 14639−14648

pubs.acs.org/ac

Combined Extinction and Absorption UV−Visible Spectroscopy as a Method for Revealing Shape Imperfections of Metallic Nanoparticles

Johan Grand, Baptiste Auguié, and Eric C. Le Ru*

The MacDiarmid Institute for Advanced Materials and Nanotechnology, School of Chemical and Physical Sciences, Victoria University of Wellington, P.O. Box 600, Wellington 6140, New Zealand

Supporting Information

ABSTRACT: Metallic nanoparticle solutions are routinely characterized by measuring their extinction spectrum (with UV−vis spectroscopy). Theoretical predictions such as Mie theory for spheres can then be used to infer important properties, such as particle size and concentration. Here we highlight the benefits of measuring not only the extinction (the sum of absorption and scattering) but also the absorption spectrum (which excludes scattering) for routine characterization of metallic nanoparticles. We use an integrating sphere-based method to measure the combined extinction−absorption spectra of silver nanospheres and nanocubes. Using a suite of electromagnetic modeling tools (Mie theory, *T*-matrix, surface integral equation methods), we show that the absorption spectrum, in contrast to extinction, is particularly sensitive to shape imperfections such as roughness, faceting, or edge rounding. We study in detail the canonical case of silver nanospheres, where small discrepancies between experimental and calculated extinction spectra are still common and often overlooked. We show that this mismatch between theory and experiment becomes much more important when considering the absorption spectrum and can no longer be dismissed as experimental imperfections. We focus in particular on the quadrupolar localized plasmon resonance of silver nanospheres, which is predicted to be very prominent in the absorption spectrum but is not observed in our experiments. We consider and discuss a number of possible explanations to account for this discrepancy, including changes in the dielectric function of Ag, size polydispersity, and shape imperfections such as elongation, faceting, and roughness. We are able to pinpoint faceting and roughness as the likely causes for the observed discrepancy. A similar analysis is carried out on silver nanocubes to demonstrate the generality of this conclusion. We conclude that the absorption spectrum is in general much more sensitive to the fine details of a nanoparticle geometry, compared to the extinction spectrum. The ratio of extinction to absorption also provides a sensitive indicator of size for many types of nanoparticles, much more reliably than any observed plasmon resonance shifts. Overall, this work demonstrates that combined absorption−extinction measurements provide a much richer characterization tool for metallic nanoparticles.

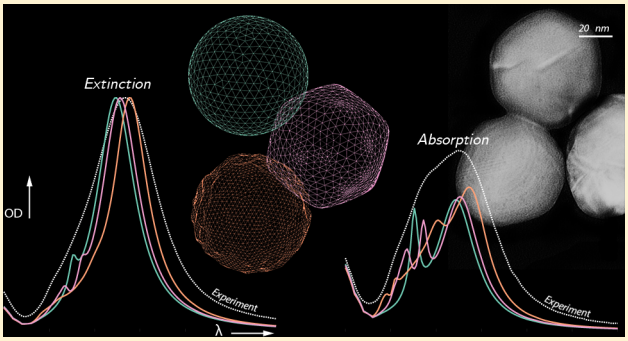

The study of the optical properties of metallic nanoparticles (NPs) began as an attempt to understand fundamental interactions between light and nanomaterials. It has now become a fruitful source of practical applications for physicists, biologists, chemists, and engineers, in fields as diverse as drug delivery,[1] nanocatalysis,[2] single-molecule detection,[3] and solar cells.[4] Following chemical or physical synthesis, NPs are usually thoroughly characterized to verify whether they will serve their intended purpose. UV−vis extinction spectroscopy is the most commonly used tool to measure their optical properties, not only because UV−vis spectrometers are readily available in most laboratories, but also because it potentially provides indirect information such as size, size distribution, state of aggregation, and NP concentration.[5] For this, the spectra must be compared to theoretical predictions. The optical properties of spheres and spherical nanoshells can be modeled accurately using Mie theory,[6,7] which solves analytically the electromagnetic scattering problem. For more general nanoparticle shapes, numerical methods such as the finite-difference time domain (FDTD) method,[8] finite-element method (FEM),[9] or discrete dipole approximation (DDA)[10,11] can be used. Accuracy may be difficult to establish with these methods as the finesse of the mesh and/or the size of the bounding box may result in errors.[12−14] More advanced approaches such as the *T*-matrix[15−17] or the surface integral equation (SIE)[18,19] methods provide more accurate and efficient predictions but are more complicated to implement. It is also worth noting that accurate and simpler approximations exist for NPs that are small enough (typically under 100 nm) in the case of nanospheres and nanoshells,[20] nanospheroids,[21] and even more complex

Received: August 20, 2019
Accepted: October 17, 2019
Published: October 17, 2019

DOI: 10.1021/acs.analchem.9b03798
Anal. Chem. 2019, 91, 14639−14648

shapes.[22] To date, the vast majority of experimental UV−vis spectra have been explained or reproduced using theoretical or numerical predictions, even for relatively complex shapes.[23−29] Any discrepancy is usually attributed to size distribution (for ensemble measurements),[5] minor changes in the geometric parameters (which are not always known accurately),[30,31] or uncertainties in the metal dielectric function.[32] With such practical limitations in characterizing precisely the samples, the overall fair agreement between theory and experiment suggests that the extinction spectrum does not in fact strongly constrain the nanoparticle properties. We will demonstrate below that absorption spectroscopy can provide much tighter constraints on the precise shape of metal nanoparticles.

Standard UV−vis spectroscopy measures transmission over a fixed path length (typically 1 cm), from which the extinction spectrum can be inferred (Beer's law). Although sometimes called an absorption spectrum, it is in fact extinction that is measured—the sum of absorption and scattering of light by the NPs. These two processes are fundamentally different and thus provide different insights into the NPs' interaction with light. Depending on the application, one may want to exploit one property over the other, for example, absorption for photothermal therapy,[33] and extinction for plasmonic sensors.[34] Absorption dominates for small NPs, and scattering for large NPs, but for intermediate sizes (in the range of 40−100 nm), absorption and scattering can be of a similar order of magnitude.[7] Some relevant information on the NPs may then be missed by measuring only the extinction spectrum. However, because of the relative difficulty in measuring absorption spectra, little effort has been dedicated to exploiting both extinction and absorption spectra for nanoparticle characterization. Over 30 years ago, Kreibig et al.[35] used photothermal spectroscopy to show that the two spectra were indeed different. More recently, such measurements have been further improved to measure the absorption spectrum of a single nanoparticle.[36−38] This approach is, however, not practical for nanoparticle routine characterization. A simpler method based on measuring scattering at 90° has also been proposed,[39,40] but inferring the absorption from it remains very approximate. A more appealing alternative, similar to standard UV−vis in many respects, is to place the sample solution inside an integrating sphere and deduce its absorption from a measurement of the sphere throughput.[41] This method has been primarily used in the context of seawater measurements,[42−44] with only sporadic reports of its application to NPs.[45,46] With careful calibration,[47,48] the absolute scattering-independent absorption spectrum can be retrieved, and the scattering spectrum can then be obtained by subtraction from the extinction spectrum. This was measured in ref 45 for silver nanospheres over a wide range of sizes between 30 and 140 nm, but only an approximate calibration was applied to obtain absolute absorption spectra and no comparison was attempted with theory.

Here we show that an integrating sphere-based measurement of both absorption and extinction UV−vis spectra provides much more insight into the NP properties than the standard extinction-only measurement. We focus in particular on a well-tested system that is used in many applications: 60 nm citrate-coated silver nanospheres dispersed in water. Similar NPs have been used in a number of contexts including surface-enhanced Raman spectroscopy,[49] single-molecule detection,[50−52] surface-enhanced fluorescence,[53] and molecule−plasmon resonance coupling.[46] We show that, while the experimental extinction matches to some extent the theoretical predictions, the absorption spectrum does not, neither in absolute intensity nor in spectral shape. To further investigate these large discrepancies, we use a suite of accurate electromagnetic calculation tools, including the Mie theory,[7] the *T*-matrix method,[16] and the surface integral equation method.[18] By comparing these predictions to our experiments, we discuss possible explanations including the choice of Ag dielectric function, the elongation of the NP, faceting, and surface roughness. We conclude that these factors typically have a much more pronounced effect on the absorption spectrum than on extinction, emphasizing the importance of the former for routine NP characterization. We also show that the ratio of extinction to absorption provides a strong constraint on the nanoparticle size. Finally, examples of combined absorption/extinction measurements for nonspherical particles, namely, silver nanocubes, are also given to further assert the generality of these conclusions. The extension of this approach to gold nanoparticles is also discussed.

EXPERIMENTAL RESULTS

Comparisons between experimental and predicted absorption, extinction, and scattering spectra are shown in Figure 1 in the case of 60 nm radius Ag nanospheres dispersed in water. In the case of extinction, the agreement between theory and experiment is reasonable but far from perfect. The position of the main dipolar localized surface plasmon (LSP) resonance is predicted at 423 nm and observed at 433 nm. Theory predicts a small peak associated with the quadrupolar LSP at 377 nm, which is not visible in the experiment. The experimental spectrum is also broader than the theoretical one. The latter can, however, be partly explained by taking into account the unavoidable NP size distribution. This is also shown in Figure 1 for the size distribution based on transmission electron microscopy (TEM) analysis (provided by the NP manufacturer), which explains to some extent the broadening. The remaining discrepancy may be attributed to a number of factors including shape distribution, dielectric function, etc., but lacks distinct spectral features to allow for further investigations.

The situation is quite different for the absorption spectrum, where predictions and observations differ significantly in at least two key aspects. First, theory predicts a prominent peak at 377 nm corresponding to the quadrupolar plasmon resonance of the sphere. This remains even for large size distribution (even much larger than shown in the figure) but is not observed experimentally. Second, the absolute absorbance is much larger than predicted, by as much as a factor of 2 in parts of the spectrum. The NP concentration is here fixed to match the intensity of the extinction spectrum and cannot therefore be adjusted to correct this problem. As a result, the observed scattering spectrum is less intense than predicted. The spectral shape is, however, similar to predictions, as the quadrupolar resonance is barely visible in scattering.

In contrast to extinction, these discrepancies in absorption are now too large to be ignored. Understanding their origin might not only improve theoretical predictions of NP optical properties but also help obtain rapid feedback for NP synthesis. In the rest of this paper, we will review and discuss the most likely causes of these discrepancies focusing first on the case of the indiscernible quadrupole resonance in the experimental absorption spectrum.

DOI: 10.1021/acs.analchem.9b03798
Anal. Chem. 2019, 91, 14639−14648

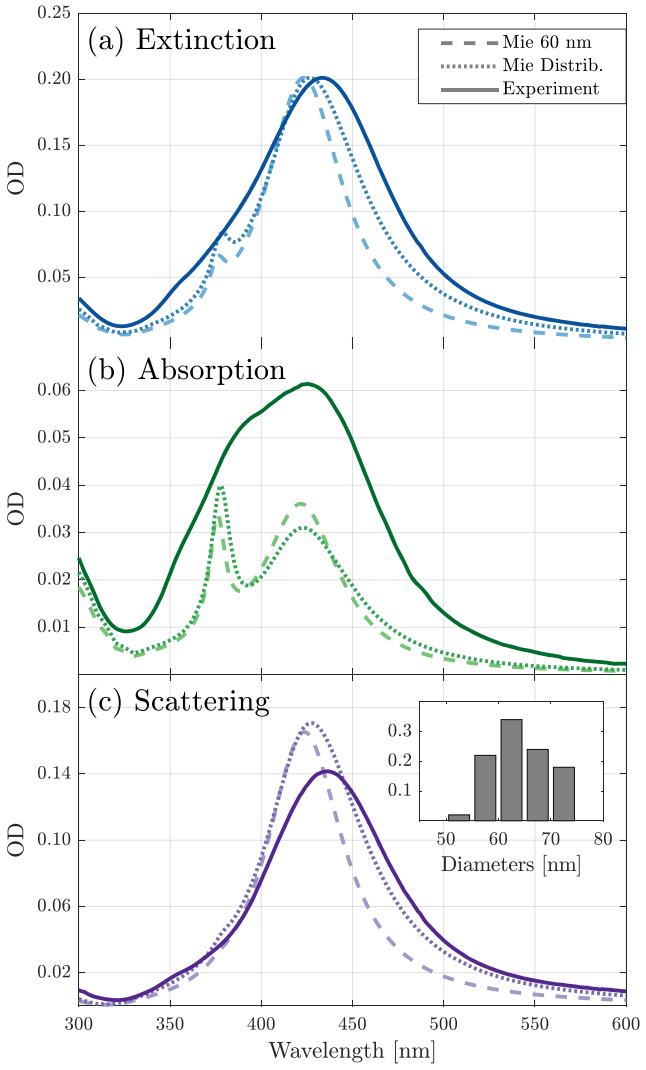

Figure 1. Extinction, absorption, and scattering spectra of a 60 nm spherical silver NP colloidal solution dispersed in water. The experimental data (solid line) is compared to the results of the Mie calculations of a single NP (dashed line) or of a collection of NPs whose size distribution matches that specified by the manufacturer (shown in the inset). In the latter case, the spectra are calculated for each size and weighted by the corresponding probabilities measured from TEM.

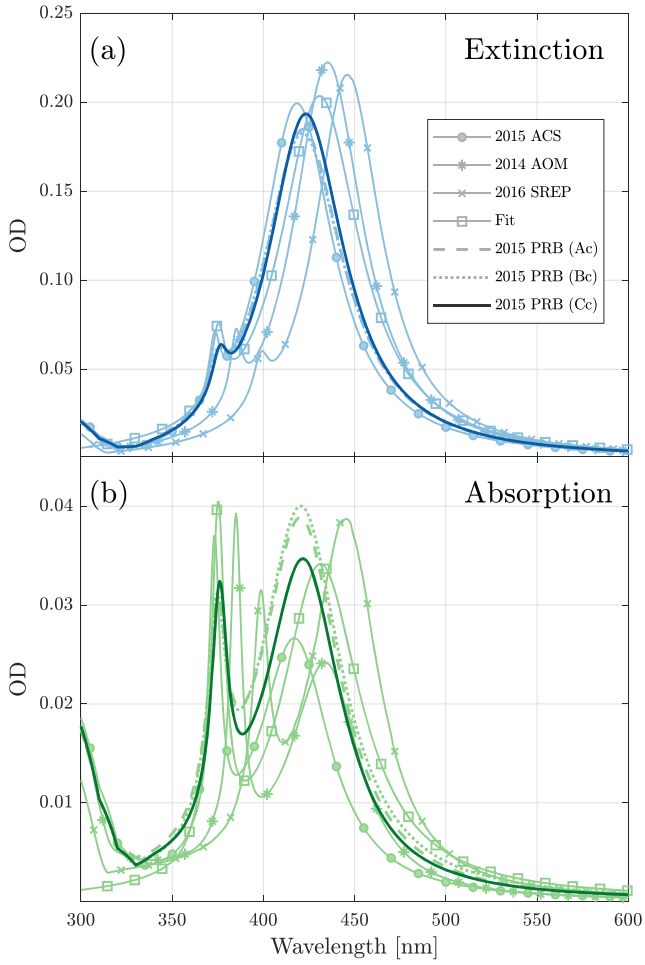

Figure 2. Single-particle extinction and absorption spectra for a 60 nm silver sphere in water, calculated using Mie theory with different sets of dielectric functions: 2015 ACS (ref 54), 2014 AOM (ref 55), 2016 SREP (ref 32), Fit (ref 56), 2015 PRB (ref 57). The latter provides three different sets of measurements and uses postprocessing to ensure Kramers–Krönig consistency (labeled Ac, Bc, Cc). The fit is based on a Drude model fit of the 1972 Johnson and Christy measurement (ref 58). The dielectric function used for all other calculations in this article is displayed as the solid line [2015 PRB (Cc)].

COMPARISON TO THEORETICAL RESULTS

Choice of Ag Dielectric Function. A key input parameter for any electromagnetic (EM) simulation involving metallic NPs, is the choice of the dielectric function of the metal. Johnson and Christy's 1972 ellipsometric measurements[58] of the dielectric function of silver, or analytical fits based on them,[8,56,59] are often used. However, several updated measurements of the dielectric function of the most commonly used metals in plasmonics have recently appeared in the literature.[32,54,55,57,60,61] These show that Johnson and Christy's data are often inadequate to describe nanoparticles, in particular for silver. Defining a unique dielectric function for metals is indeed difficult, as it can depend on how a particular sample is fabricated. For example, roughness and crystallinity are factors that can greatly influence the optical response of a metal, and therefore its dielectric function.[57] Using the Mie theory, we plot in Figure 2 the predicted extinction and absorption properties of a 60 nm Ag sphere in water (with dielectric function taken from ref 62) with different sets of dielectric functions. The main dipolar LSP resonance can be shifted by more than 20 nm, illustrating the critical importance of the choice of the dielectric function. However, the intensity of the quadrupolar mode is relatively unaffected and remains prominent in all cases in the absorption spectrum. This uncertainty cannot therefore explain why the quadrupolar resonance is not observed experimentally. We also note that the choice of dielectric function may affect the absolute intensity of absorption. It would nevertheless not be sufficient to bridge the intensity gap between the experimental and the predicted absorption. For all the other calculations throughout the article, we chose to use the dielectric function measured and recommended by Yang et al. in ref 57 (AgC_corrected.csv, as provided in the Supporting Information of ref 57).

Particle Elongation. So far we have considered the NPs as perfect spheres, which greatly simplified the EM simulations, as Mie theory provides an analytical solution to the light

DOI: 10.1021/acs.analchem.9b03798
Anal. Chem. 2019, 91, 14639−14648

scattering problem. The assumption of an idealized spherical shape is, however, unrealistic. The simplest departure from a spherical shape is its elongation along one axis, which we investigate by considering spheroidal NPs (prolate and oblate). To model their optical response we turn to the *T*-matrix method,[15,16] an accurate, fast, and numerically stable[17] solution of the Maxwell equations, from which orientation-averaged properties can be derived with no added computational cost. As we can see in Figure 3, the dipolar resonance broadens and

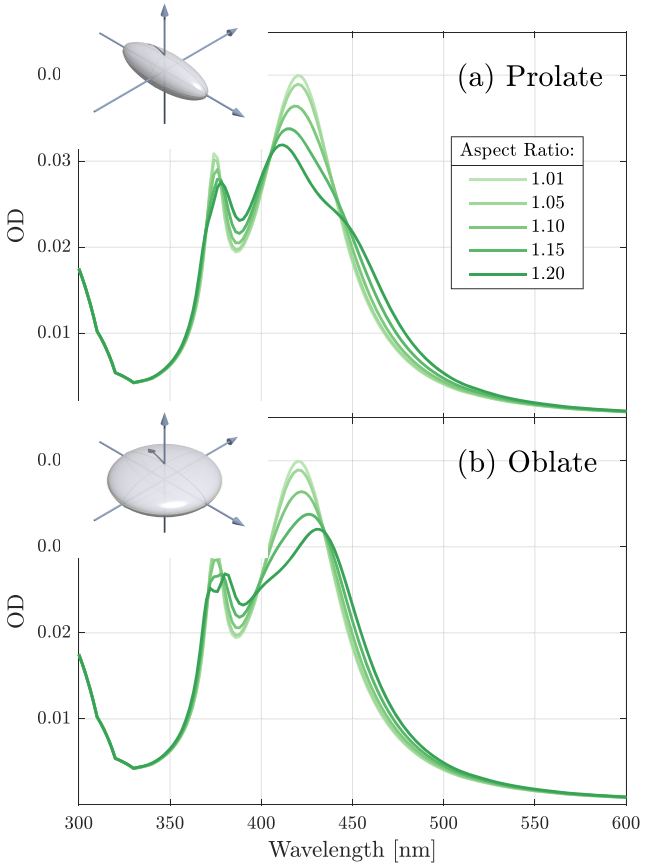

Figure 3. Absorption spectra of prolate (top panel) and oblate (bottom panel) silver NPs of different aspect ratios in water, calculated using the *T*-matrix method.

splits with the dominant peak slightly red-shifted for oblate NPs and blue-shifted for prolate NPs when the aspect ratio is increased, as is well-documented. The spectral position and relative intensity of the quadrupolar mode remains, however, largely unaffected by the change in aspect ratio. Broadening and splitting of the quadrupolar peak are only predicted to occur for aspect ratios of 1.2 and above, which is much larger than we reasonably expect in our samples. Thus, even considering a distribution of prolate and oblate NPs with different aspect ratio would fail to explain the experimental absorption spectrum.

Faceting. The shape of a NP is greatly affected by its crystalline structure, which governs the growth mechanisms and generates faceted particles; imperfections in growth can lead to particles with different number or types of facets.[63] Although evident in TEM images of nanospheres, especially for silver (see, for example, the inset in Figure 4), facets are usually ignored in theoretical predictions for spherical NPs because of

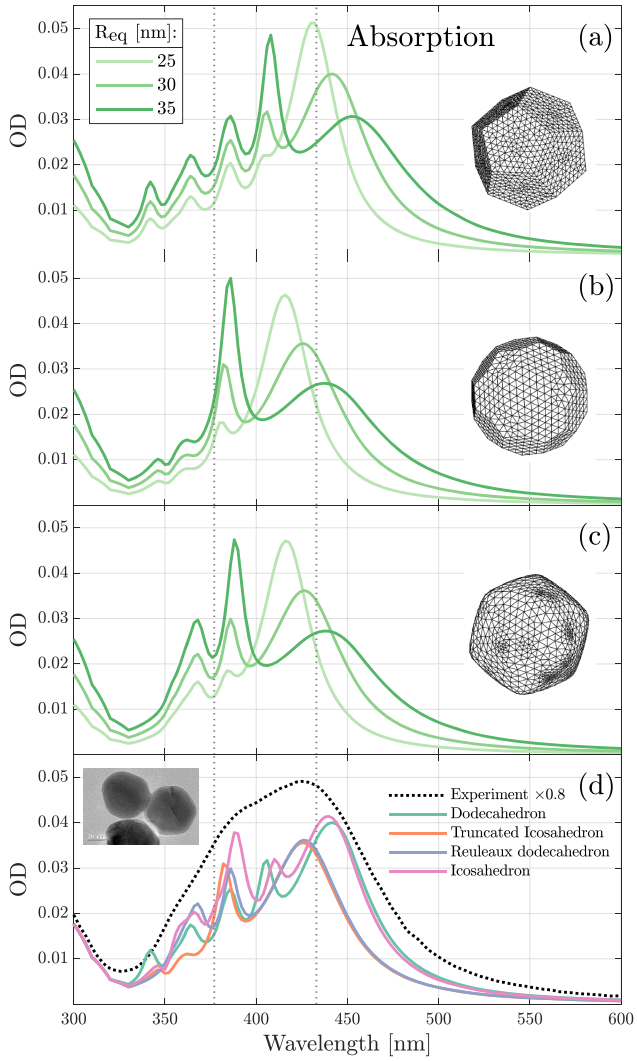

Figure 4. Absorption spectra of three different silver NPs in water calculated by SIE: a dodecahedron (a), a truncated icosahedron (b), and a Reuleaux dodecahedron (c). The three spectra on each panel correspond to different particle sizes, as characterized by the radius of the equivalent-volume sphere (R_{eq} from 25 to 35 nm). In the bottom panel (d), we superimpose the absorption spectra of different-shaped particles of the same volume (R_{eq} = 30 nm) together with the scaled experimental spectrum. The inset shows a TEM image provided by the manufacturer (Nanocomposix) of the 30 nm radius Ag nanospheres used for the experiment.

the added complexity. To predict the optical properties of faceted NPs we use the SIE method, which has been shown to be particularly accurate for plasmonic NPs of arbitrary shapes.[18,19,64] SIE allows modeling of any kind of particle shape by meshing its surface. It presents many advantages over other commonly used numerical methods discretizing the entire volume of a nanoparticle, such as DDA, finite difference time-domain, or finite element methods. SIE does not require any bounding box to surround the particle, and only the surface is meshed, making it less demanding in computational resources than many other methods. Orientation averaging can also be carried out without a significant increase in computing time. We have considered many different types of faceted NPs and show in Figure 4 the absorption spectra predicted for representative cases: dodecahedra (20 faces), truncated icosahedra (32 faces), and Reuleaux dodecahedra (12 curved

DOI: 10.1021/acs.analchem.9b03798
Anal. Chem. 2019, 91, 14639−14648

faces) of different sizes. Note that all SIE calculated spectra presented here are averaged over 200 NP orientations to be more representative of the experimental conditions (we recall that the sample is a colloidal suspension of NPs in water). While this selection of shapes is unlikely to be representative of actual NP geometries—which result from complex growth mechanisms, and where facets reflect the underlying crystalline structure of the material—the simulation results suggest general conclusions that do not depend on the particular arrangement of facets, only the departure from sphericity.

We observe that faceting introduces new resonances in the optical response of the NPs, which appear in the sphere's quadrupole resonance region. Remarkably, the NP size only affects the position of the main dipolar resonance (longest wavelength), not that of the extra resonances. Nevertheless, shape does affect the exact position of these resonances, and as illustrated in Figure 4d, a distribution of differently faceted shapes could contribute to washing out the prominent quadrupolar peak predicted for perfect spheres. This would require relatively strong faceting (for example, for a dodecahedron), but is not incompatible with the uneven shapes observed in TEM images (inset of Figure 4d). We therefore conclude that some degree of random faceting could explain at least to some extent the broad and almost featureless experimental absorption spectrum.

Surface Roughness. A final source of nonsphericity that we will discuss here is surface roughness. As for the case of NP faceting, many studies on the effect of NP surface roughness on plasmon resonance have been published,[65−67] with different and sometimes contradicting conclusions.[31,68] We do not intend here to give a definitive conclusion on the effect of surface roughness on the optical properties of NPs, as it may depend on a number of factors like the NP shape, size, material, detailed type of roughness, etc. Most studies, however, rely on the comparison between calculations and experimental extinction or scattering spectra alone. Having access to all the far-field optical properties of the NPs provides additional insight and sharpens the conclusions drawn from the comparison with calculations.

We considered roughened spheres with random uncorrelated perturbations of the surface mesh and modeled their optical properties using SIE. The degree of roughness can be characterized by the root-mean-square (rms) average of the local radius deviation (measured from the center of the sphere), denoted δr. We present in Figure 5 calculations for spheres of average radius 30 nm and rms roughness δr ranging from 0 (sphere) to 1.4 nm. Roughness induces a red-shift in the plasmon resonance positions, both dipolar and quadrupolar, which is observed in extinction, scattering, and absorption. For the highest roughness considered in this simulation (1.4 nm rms, still within a realistic range), the quadrupolar resonance has broadened to the point where it is no longer prominent in the absorption spectrum and appears as a small shoulder peak. It has also shifted substantially to lie in the middle of the dipole and quadrupole resonance of the perfect sphere. Because this shift strongly depends on the degree of roughness, a distribution of rms roughness could easily broaden and wash out the quadrupole peak to the point where it is no longer visible in absorption. This would also have a limited, hardly detectable impact on the extinction spectrum, as can be inferred from Figure 5. These predictions suggest that surface roughness may also play a role in explaining the experimental absorption spectrum, in addition

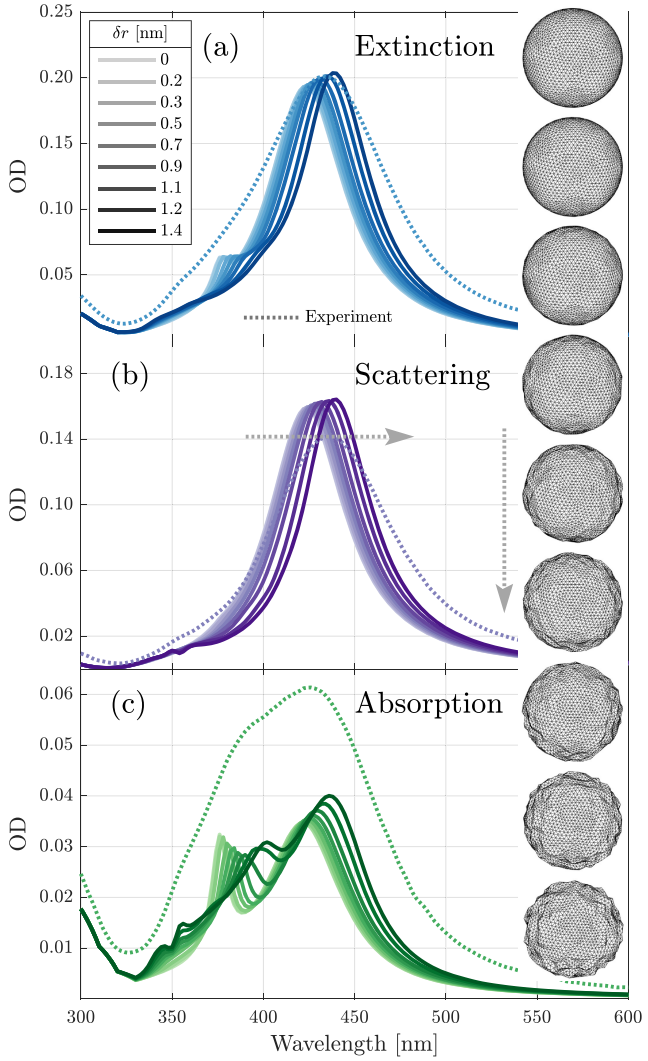

Figure 5. Predicted (from SIE) extinction, scattering, and absorption spectra of spherical silver NPs of different rms roughnesses δr. The NPs are in water and have the same volume as a 60 nm sphere. In each panel, the experimental spectrum is plotted in dotted lines.

to the more easily identifiable faceting discussed earlier. By inspection of Figures 4 and 5, it appears that disentangling these two effects will be difficult purely from far-field measurements. Nevertheless, the spectra in Figures 4 and 5 demonstrate how sensitive the entire absorption spectrum is to small changes on the particle surface (faceting and roughness), in contrast to the extinction and scattering spectra, which barely change except for the dipolar resonance. It is also worth pointing out that, although outside our scope here, it would be interesting to further test the predictions of Figure 5 experimentally using nanoparticles of varying roughness, for example, using chemical etching.

Absolute Absorption Intensity. We now come back to our second main observation: the measured absorption spectrum appears much more intense than predicted. In fact, we can see from the results of Figures 3−5 that shape imperfections may affect the spectral profile, but not much the overall absorption intensity. Although the NP concentration can be used to scale the predicted spectra, it will scale both extinction and absorption, so it cannot explain this discrepancy. In order to take the NP concentration out of

DOI: 10.1021/acs.analchem.9b03798
Anal. Chem. 2019, 91, 14639−14648

the equation, it is convenient here to consider the ratio η of extinction to absorption. We plot the experimental ratio η in Figure 6, alongside a selection of theoretical predictions. The

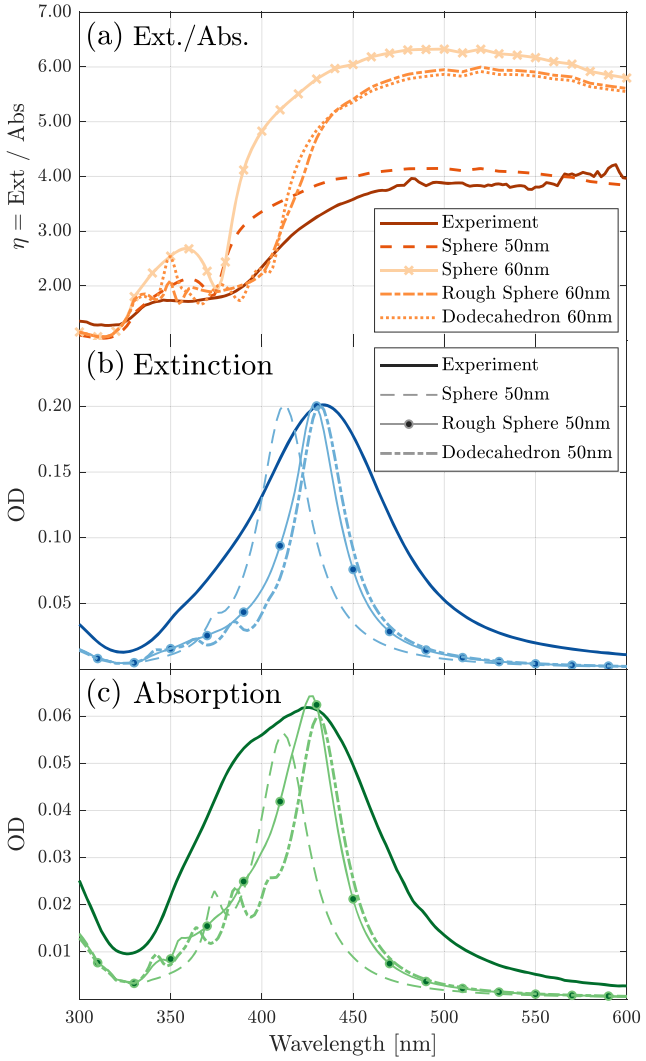

Figure 6. Top panel: ratio of extinction to absorption spectra for our measured NPs (solid line) along with a number of representative predictions for 50 and 60 nm spheres, a 60 nm roughened sphere (δr = 1.4 nm), and a dodecahedron (radius of the equivalent-volume sphere, 60 nm). Middle and bottom panels: extinction and absorption spectra for a 50 nm sphere, a rough sphere (δr = 1.4 nm), and a dodecahedron compared to experiments (solid lines).

main discrepancy between experiment and theory is observed in the region above 420 nm, i.e., at the dipolar resonance and beyond. The ratio η is approximately constant in this region, around 4 in the experiments, but stays around 6 for predictions with 60 nm NP spheres, even faceted or roughened (keeping the volume-equivalent diameter at 60 nm). In all our calculations, we found that the most important factor for the extinction to absorption ratio in this region is the particle size, as quantified using the NP volume V or the volume-equivalent diameter. This is an important observation as this ratio then provides a sensitive measure of nanoparticle volume independent of shape. This can be explained in the dipolar approximation, where absorption is proportional to V, while scattering is proportional to V^2: one therefore expects $\eta - 1$ to be proportional to V.

We can push predictions for η down to ~4 simply by decreasing the particle size down to 50 nm, independent of shape imperfections. This results in a concomitant blue-shift of the plasmon resonance, which for perfect spheres no longer matches the predictions (Figure 6). However, as discussed earlier, roughness and faceting are accompanied by a red-shift of the resonance, which can in fact compensate the size-induced blue-shift. This is shown in Figure 6: smaller 50 nm NPs with sufficient roughness or faceting have similar dipolar resonance to a 60 nm perfect sphere and can therefore not only match the observed resonances but also the absolute intensities of both extinction and absorption spectra. Such sizes are still compatible with size estimates from TEM images, because a 50 nm volume-equivalent diameter corresponds to larger cord dimensions: the largest cord ("diameter") for a 50 nm dodecahedron, for example, is of the order of 56 nm. Failure to account for these shape effects, which are not observable in extinction, results in a large overestimation of the particle volume: a 60 nm volume-equivalent radius instead of 50 nm corresponds to a 70% error. More importantly, a similarly large error would result in any estimate of the derived particle concentration from the intensity of the extinction spectrum. Such a large error would have important implications in most contexts.

It is also worth pointing out here that the extinction to absorption ratio will also be particularly relevant to any type of nanoparticles, not just silver or even metallic ones, as it is always highly sensitive to size except for the smallest sizes (typically smaller than 10 nm diameter). This is illustrated in Figure 7 for the important case of gold nanoparticles. Inferring the size from the extinction spectrum can be difficult, as the spectrum (once normalized in intensity) barely changes with diameter, especially between 10 and 30 nm (Figure 7a). The absorption spectral shape also hardly changes (not shown), but the ratio $\eta(\lambda)$ does vary significantly (Figure 7b), and therefore provides a robust experimental tool to determine gold NP size.

Finally, it is also worth highlighting that a large size distribution will have a different effect on absorption than on extinction. The latter is proportional to V^2 through the scattering contribution and will therefore be more dominated by larger NP (relative to absorption). The extinction spectrum would then be red-shifted compared to the absorption spectrum, although this is likely observable only for relatively large size distribution.

Nonspherical Nanoparticles. To show that the results and discussion presented so far are more general than for just spherical nanoparticles, we conclude by considering non-spherical nanoparticles. We focus in particular on 100 nm silver nanocubes.[69] Their orientation-averaged optical properties can again be predicted using SIE and compared to experiments as summarized in Figure 8. As previously reported,[24,26,29] the extinction spectrum is a lot richer than that for spheres, with a broad dipolar resonance at ~570 nm and at least three additional higher energy peaks corresponding to higher-order resonances. As for spheres, the higher-order resonances are much more prominent in the absorption spectrum, which facilitates their study and comparison with theory. We also note that the dipolar resonance is almost absent from the absorption spectrum; therefore, a combined extinction−absorption study is needed to maximize our experimental input. The predicted spectra for a 100 nm nanocube exhibit similar resonances in both extinction and absorption, but they are all significantly red-shifted compared to experiment. We

DOI: 10.1021/acs.analchem.9b03798
Anal. Chem. 2019, 91, 14639−14648

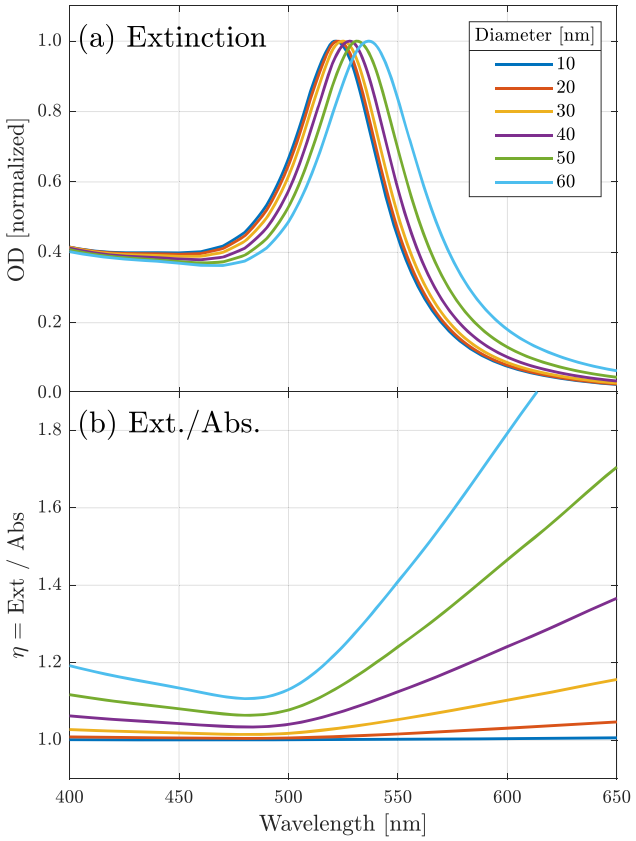

Figure 7. Predicted extinction spectra (a) and extinction to absorption ratios (b) for gold nanospheres of varying diameter in water, calculated using Mie theory and the gold dielectric function from ref 60.

would have to bring the edge dimension down to 80 nm to correct this, but this is unrealistic given the TEM images (see inset). We instead consider shape imperfections, as for sphere, and in particular the rounding of the edges and corners, which is in fact apparent in the TEM image. This is accounted for by introducing a fillet on each edge as shown in Figure 8. This rounding results in a blue-shift of all the resonances and with fillets between 10 and 14 nm; several resonances can match the experiments, but not quite all. This can be further tuned by changing the size for a fixed fillet of 10 nm as shown in Figure 8b. A 93 nm edge-length nanocube with 10 nm fillet appears to provide the closer match to the experiment in resonance position and intensity for both extinction and absorption. A small size distribution could explain the observed broader dipolar resonance in extinction. The remaining discrepancy is mostly in the absorption intensity of the ∼475 nm peak, and addressing it would require a more accurate model of the particle geometry. This mode is associated with strong field enhancements in the corners,[29] and we expect that predicting the its absorption more accurately will require using a different fillet size for corners than for edges. That the fine details of the particle's morphology can have notable effects in the absorption spectrum presents both a challenge—requiring finer shape characterization—and an opportunity: very accurate information on the nanometer scale can be obtained by far-field optical measurements.

CONCLUSION

This work demonstrates the benefits of measuring both extinction and absorption spectra for routine characterization of metallic nanoparticles in solution. While the main dipolar resonance is most visible in extinction, we have showed that the higher-order resonances are much more prominent in absorption. We moreover highlighted that these higher-order resonances are particularly sensitive to small imperfections in NP shape, such as faceting and roughness. As a result, many theoretical fits that were acceptable for extinction are not compatible with the experimental absorption spectrum. Fitting the latter introduces much tighter constraints on the NP geometry, notably the inclusion of roughness and/or faceting.

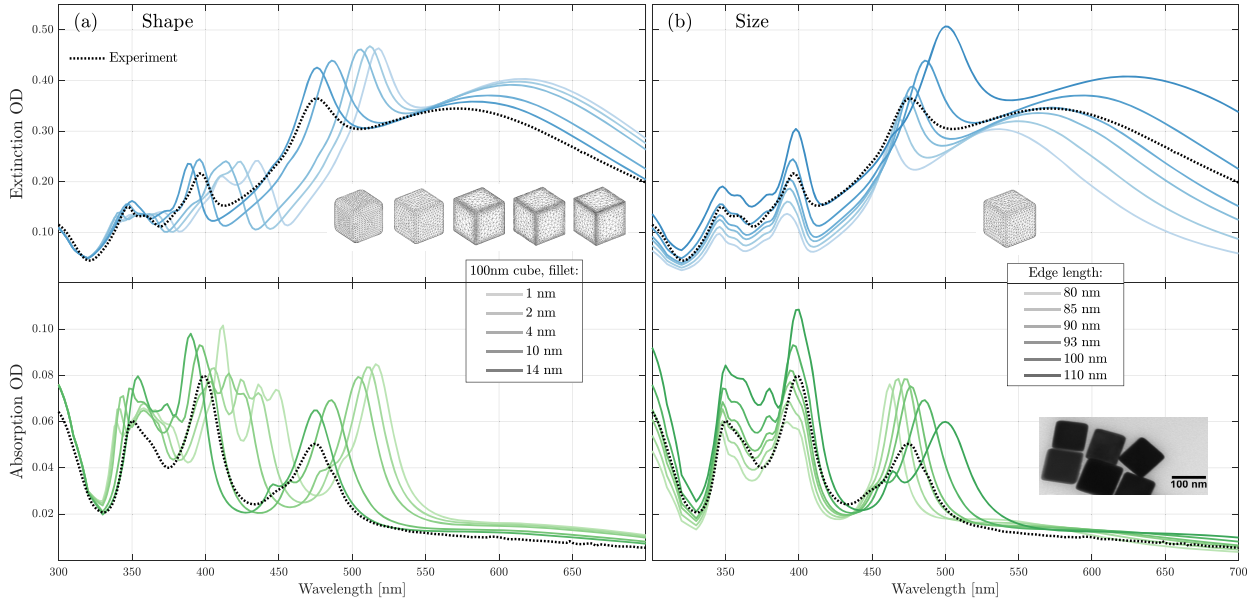

Figure 8. (a) SIE calculated extinction (top) and absorption (bottom) spectra of 100 nm nanocubes with different sizes of fillet applied to all edges. (b) Same as panel a but the cube fillet is fixed at 10 nm and the volume of the cube is varied. In all the panels, the experimental spectra are plotted in dashed lines.

DOI: 10.1021/acs.analchem.9b03798
Anal. Chem. 2019, 91, 14639−14648

The ratio of extinction to absorption also provides an additional experimental constraint, which is primarily dictated by the overall particle size, not its shape. We have applied these considerations to the canonical system of 60 nm diameter silver nanospheres and showed that the experimental absorption could only be explained by invoking roughness and faceting. This in turn explains the long-standing puzzle that the quadrupolar resonance is barely observed in the extinction spectrum despite its large prominence in theoretical predictions. It also suggests that large errors in estimated NP volume and concentration may arise when inferring them from the extinction spectrum only. Similar considerations were then applied to silver nanocubes, where the importance of rounding the edges was highlighted. Interestingly, in both cases, the spectra and the ratio of extinction to absorption can all be explained using reported bulk dielectric function for silver, which suggests that there is no need to modify it to account for additional losses due to polycrystallinity or other defects in nanoparticles. We believe this approach is generally applicable to many types of nanoparticles. For the smallest sizes (typically less than 20 nm), scattering is negligible, and the absorption spectrum will not add extra insight. But for anything larger, the combination of extinction−absorption spectra provides a much richer, yet simple and easily accessible, characterization of the NP properties. Even for large NPs like the 100 nm nanocubes where scattering dominates, the weaker absorption spectrum still provides more detailed information than the extinction spectrum. These benefits could moreover extend to the characterization of capping molecules adsorbed on the surface of the NPs, which, like roughness, should affect absorption much more than extinction. We believe this approach can be applied to many related systems including dye-coated metallic nanoparticles, for the study of weak and strong plasmon−molecule resonance coupling, and other types of nonmetallic nanoparticles and microparticles where both absorption and scattering are typically present.

METHODS

Nanoparticles. The 60 nm citrate-stabilized silver nanoparticles were obtained from Nanocomposix (U.S.A.). The size distribution is provided by the manufacturer. The stock NP colloidal suspension was diluted by a factor of 10 for the measurements. The 100 nm poly(vinylpyrrolidone) (PVP)-coated silver nanocubes (NanoXact) were also obtained from Nanocomposix (U.S.A.). The 100 nm diameter carboxyl-coated amorphous silica sphere were obtained from Micromod (Germany).

Absorption/Extinction Measurements. We recorded the optical properties of the Ag NP solution using the CloudSpec-UV-v0.8 from Marama Laboratories (New Zealand). This instrument uses an integrating sphere to measure both extinction and absorption spectra of samples. Both are given in units of cm^{-1}, i.e., in optical density normalized to a path length of 1 cm. The scattering spectrum can, therefore, be deduced from the difference of both. To check the validity of these spectra, we performed a series of measurements of the eosin B dye as a function of concentration in water (nonscattering samples). These tests (see Figure S1) confirmed that the extinction and absorption spectra were the same and were linear over the concentration range of interest. Similar measurements were then carried out in the presence of scattering by adding 300 nm diameter carboxyl-coated silica spheres (whose concentration was adjusted to match the Ag NP scattering at resonance). The absorption spectra were the same as those measured in the absence of scattering in water, as expected, see Figure S1. Finally, measurements on the NPs were performed for three dilution factors, namely, 5, 10, and 40, and gave the same spectrum when adjusted by the corresponding factor (see Figure S2).

Mie Theory. Mie theory calculations were performed using the SPlaC package.[56,70] In all EM calculations, the wavelength-dependent refractive index for water was taken from ref 71. Except where specified in the main text, the dielectric function for silver were taken from ref 57 (sample C, AgC_corrected.csv, as provided in the Supporting Information of ref 57).

Calculations on Elongated NPs. The optical properties of spheroidal NPs were computed using SMARTIES,[72] which provides a Matlab implementation of the *T*-matrix method with recently developed improved algorithms specially developed for spheroidal nanoparticles.[73,74] An estimate of the accuracy of the results is returned by the computation, and high accuracy (comparable to Mie theory, better than 10^{-12})[17] is achieved for all the examples considered here.

Surface Integral Equation Calculations. For other nonspherical particles, the surface integral equation formalism was used.[18,64] We have used an implementation specially developed (and tested) for plasmonics and metallic nanoparticles.[19] The quality of the mesh in each case is illustrated in the corresponding figures. To create the roughened sphere, we started from a coarse mesh of 630 nodes, and for each node, the distance from the origin was multiplied by a factor $1 + \kappa u$, where u is a random number between −1 and 1. The degree of roughness can be adjusted by changing κ. The resulting mesh was then further refined (2514 nodes) to improve the accuracy of the calculation. We checked that the predicted spectra were almost identical for two different roughened sphere generated with the same κ.

ASSOCIATED CONTENT

Supporting Information

The Supporting Information is available free of charge on the ACS Publications website at DOI: 10.1021/acs.analchem.9b03798.

Additional figures confirming the validity of the scattering-independent absorption spectra (PDF)

AUTHOR INFORMATION

Corresponding Author

*E-mail: eric.leru@vuw.ac.nz.

ORCID

Baptiste Auguié: 0000-0002-2749-5715

Eric C. Le Ru: 0000-0002-3052-9947

Notes

The authors declare the following competing financial interest(s): The instrument used for the measurements discussed in this manuscript was developed and is commercialized by Marama Labs, a start-up company that was spun out from our research. As a consequence, two of the authors (B.A. and E.C.L.R.) have a small share in this company.

ACKNOWLEDGMENTS

The authors thank the Royal Society Te Apārangi for support through a Rutherford Discovery Fellowship (B.A.) and a

DOI: 10.1021/acs.analchem.9b03798
Anal. Chem. 2019, 91, 14639−14648

Marsden Grant (J.G. and E.C.L.R.). We are grateful to Marama Laboratories Ltd. for providing us early access to their prototype instrument. We are grateful to Nanocomposix for providing us with silver nanocubes.

REFERENCES

(1) Patra, J. K.; Das, G.; Fraceto, L. F.; Campos, E. V. R.; Rodriguez-Torres, M. d. P.; Acosta-Torres, L. S.; Diaz-Torres, L. A.; Grillo, R.; Swamy, M. K.; Sharma, S.; Habtemariam, S.; Shin, H.-S. *J. Nanobiotechnol.* **2018**, *16*, 71.
(2) Rodrigues, T. S.; da Silva, A. G. M.; Camargo, P. H. C. *J. Mater. Chem. A* **2019**, *7*, 5857−5874.
(3) Le Ru, E. C.; Etchegoin, P. G. *Annu. Rev. Phys. Chem.* **2012**, *63*, 65.
(4) Mubeen, S.; Lee, J.; Lee, W.-r.; Singh, N.; Stucky, G. D.; Moskovits, M. *ACS Nano* **2014**, *8*, 6066−6073.
(5) Haiss, W.; Thanh, N. T. K.; Aveyard, J.; Fernig, D. G. *Anal. Chem.* **2007**, *79*, 4215−4221.
(6) Mie, G. *Ann. Phys.* **1908**, *330*, 377−445.
(7) Bohren, C. F.; Huffman, D. R. *Absorption and Scattering of Light by Small Particles*; John Wiley & Sons Inc.: New York, 1983.
(8) Hao, F.; Nordlander, P. *Chem. Phys. Lett.* **2007**, *446*, 115−118.
(9) Khoury, C. G.; Norton, S. J.; Vo-Dinh, T. *ACS Nano* **2009**, *3*, 2776−2788.
(10) Yang, W.-H.; Schatz, G. C.; Van Duyne, R. P. *J. Chem. Phys.* **1995**, *103*, 869−875.
(11) Yurkin, M.; Hoekstra, A. *J. Quant. Spectrosc. Radiat. Transfer* **2011**, *112*, 2234−2247.
(12) Hoffmann, J.; Hafner, C.; Leidenberger, P.; Hesselbarth, J.; Burger, S. *Proc. SPIE* **2009**, 73900J.
(13) Lesina, A. C.; Vaccari, A.; Berini, P.; Ramunno, L. *Opt. Express* **2015**, *23*, 10481−10497.
(14) Kupresak, M.; Zheng, X.; Vandenbosch, G. A. E.; Moshchalkov, V. V. *Opt. Express* **2017**, *25*, 26760−26780.
(15) Waterman, P. C. *Proc. IEEE* **1965**, *53*, 805−812.
(16) Mishchenko, M. I.; Travis, L. D.; Lacis, A. A. *Scattering, Absorption and Emission of Light by Small Particles*, 3rd ed.; Cambridge University Press: Cambridge, U.K., 2002.
(17) Somerville, W. R. C.; Auguié, B.; Le Ru, E. C. *J. Quant. Spectrosc. Radiat. Transfer* **2015**, *160*, 29−35.
(18) Kern, A. M.; Martin, O. J. F. *J. Opt. Soc. Am. A* **2009**, *26*, 732−740.
(19) Raziman, T. V.; Somerville, W. R. C.; Martin, O. J. F.; Le Ru, E. C. *J. Opt. Soc. Am. B* **2015**, *32*, 485.
(20) Schebarchov, D.; Auguié, B.; Le Ru, E. C. *Phys. Chem. Chem. Phys.* **2013**, *15*, 4233−4242.
(21) Majic, M. R. A.; Pratley, L.; Schebarchov, D.; Somerville, W. R. C.; Auguie, B.; Le Ru, E. C. *Phys. Rev. A: At., Mol., Opt. Phys.* **2019**, *99*, 013853.
(22) Yu, R.; Liz-Marzán, L. M.; García de Abajo, F. J. *Chem. Soc. Rev.* **2017**, *46*, 6710−6724.
(23) Russell, B. K.; Mantovani, J. G.; Anderson, V. E.; Warmack, R. J.; Ferrell, T. L. *Phys. Rev. B: Condens. Matter Mater. Phys.* **1987**, *35*, 2151−2154.
(24) Sherry, L. J.; Chang, S.-H.; Schatz, G. C.; Van Duyne, R. P.; Wiley, B. J.; Xia, Y. *Nano Lett.* **2005**, *5*, 2034−2038.
(25) Tao, A.; Sinsermsuksakul, P.; Yang, P. *Angew. Chem., Int. Ed.* **2006**, *45*, 4597−4601.
(26) McMahon, J. M.; Wang, Y.; Sherry, L. J.; Van Duyne, R. P.; Marks, L. D.; Gray, S. K.; Schatz, G. C. *J. Phys. Chem. C* **2009**, *113*, 2731−2735.
(27) Rodríguez-Fernández, J.; Novo, C.; Myroshnychenko, V.; Funston, A. M.; Sánchez-Iglesias, A.; Pastoriza-Santos, I.; Pérez-Juste, J.; García de Abajo, F. J.; Liz-Marzán, L. M.; Mulvaney, P. *J. Phys. Chem. C* **2009**, *113*, 18623−18631.
(28) Henry, A.-I.; Bingham, J. M.; Ringe, E.; Marks, L. D.; Schatz, G. C.; Van Duyne, R. P. *J. Phys. Chem. C* **2011**, *115*, 9291−9305.
(29) Mahmoud, M. A.; Chamanzar, M.; Adibi, A.; El-Sayed, M. A. *J. Am. Chem. Soc.* **2012**, *134*, 6434−6442.
(30) Wang, H.; Fu, K.; Drezek, R.; Halas, N. *Appl. Phys. B: Lasers Opt.* **2006**, *84*, 191−195.
(31) Trügler, A.; Tinguely, J.-C.; Krenn, J. R.; Hohenau, A.; Hohenester, U. *Phys. Rev. B: Condens. Matter Mater. Phys.* **2011**, *83*, 081412.
(32) Jiang, Y.; Pillai, S.; Green, M. A. *Sci. Rep.* **2016**, *6*, 30605.
(33) Huang, X.; El-Sayed, I. H.; Qian, W.; El-Sayed, M. A. *J. Am. Chem. Soc.* **2006**, *128*, 2115−2120.
(34) McFarland, A. D.; Van Duyne, R. P. *Nano Lett.* **2003**, *3*, 1057−1062.
(35) Kreibig, U.; Schmitz, B.; Breuer, H. D. *Phys. Rev. B: Condens. Matter Mater. Phys.* **1987**, *36*, 5027−5030.
(36) Arbouet, A.; Christofilos, D.; Del Fatti, N.; Vallée, F.; Huntzinger, J. R.; Arnaud, L.; Billaud, P.; Broyer, M. *Phys. Rev. Lett.* **2004**, *93*, 127401.
(37) Tcherniak, A.; Ha, J. W.; Dominguez-Medina, S.; Slaughter, L. S.; Link, S. *Nano Lett.* **2010**, *10*, 1398−1404.
(38) Husnik, M.; Linden, S.; Diehl, R.; Niegemann, J.; Busch, K.; Wegener, M. *Phys. Rev. Lett.* **2012**, *109*, 233902.
(39) Micali, N.; Mallamace, F.; Castriciano, M.; Romeo, A.; Monsú Scolaro, L. *Anal. Chem.* **2001**, *73*, 4958−4963.
(40) Liu, B.-J.; Lin, K.-Q.; Hu, S.; Wang, X.; Lei, Z.-C.; Lin, H.-X.; Ren, B. *Anal. Chem.* **2015**, *87*, 1058−1065.
(41) Nelson, N. B.; Prézelin, B. B. *Appl. Opt.* **1993**, *32*, 6710−6717.
(42) Babin, M.; Stramski, D. *Limnol. Oceanogr.* **2002**, *47*, 911−915.
(43) Tassan, S.; Ferrari, G. M. *Appl. Opt.* **2003**, *42*, 4802−4810.
(44) Gaigalas, A. K.; He, H.-J.; Wang, L. *J. Res. Natl. Inst. Stand. Technol.* **2009**, *114*, 69−81.
(45) Evanoff, D. D.; Chumanov, G. *J. Phys. Chem. B* **2004**, *108*, 13957−13962.
(46) Darby, B. L.; Auguié, B.; Meyer, M.; Pantoja, A. E.; Le Ru, E. C. *Nat. Photonics* **2016**, *10*, 40−45.
(47) Villanueva, Y.; Veenstra, C.; Steenbergen, W. *Appl. Opt.* **2016**, *55*, 3030−3038.
(48) Tang, C.; Meyer, M.; Darby, B. L.; Auguié, B.; Le Ru, E. C. *Appl. Opt.* **2018**, *57*, 1581−1588.
(49) Le Ru, E. C.; Blackie, E.; Meyer, M.; Etchegoin, P. G. *J. Phys. Chem. C* **2007**, *111*, 13794−13803.
(50) Le Ru, E. C.; Meyer, M.; Etchegoin, P. G. *J. Phys. Chem. B* **2006**, *110*, 1944−1948.
(51) Blackie, E. J.; Le Ru, E. C.; Etchegoin, P. G. *J. Am. Chem. Soc.* **2009**, *131*, 14466−14472.
(52) Etchegoin, P. G.; Le Ru, E. C.; Meyer, M. *J. Am. Chem. Soc.* **2009**, *131*, 2713−2716.
(53) Galloway, C. M.; Etchegoin, P. G.; Le Ru, E. C. *Phys. Rev. Lett.* **2009**, *103*, 063003.
(54) McPeak, K. M.; Jayanti, S. V.; Kress, S. J. P.; Meyer, S.; Iotti, S.; Rossinelli, A.; Norris, D. J. *ACS Photonics* **2015**, *2*, 326−333.
(55) Rioux, D.; Vallières, S.; Besner, S.; Munõz, P.; Mazur, E.; Meunier, M. *Adv. Opt. Mater.* **2014**, *2*, 176−182.
(56) Le Ru, E. C.; Etchegoin, P. G. *Principles of Surface-Enhanced Raman Spectroscopy and Related Plasmonic Effects*; Elsevier: Amsterdam, The Netherlands, 2009.
(57) Yang, H. U.; D'Archangel, J.; Sundheimer, M. L.; Tucker, E.; Boreman, G. D.; Raschke, M. B. *Phys. Rev. B: Condens. Matter Mater. Phys.* **2015**, *91*, 235137.
(58) Johnson, P. B.; Christy, R. W. *Phys. Rev. B* **1972**, *6*, 4370−4379.
(59) Etchegoin, P. G.; Le Ru, E. C.; Meyer, M. *J. Chem. Phys.* **2006**, *125*, 164705.
(60) Olmon, R. L.; Slovick, B.; Johnson, T. W.; Shelton, D.; Oh, S.-H.; Boreman, G. D.; Raschke, M. B. *Phys. Rev. B: Condens. Matter Mater. Phys.* **2012**, *86*, 235147.
(61) Jiang, Y.; Pillai, S.; Green, M. A. *Opt. Express* **2015**, *23*, 2133−2144.
(62) Schiebener, P.; Straub, J.; Levelt Sengers, J. M. H.; Gallagher, J. S. *J. Phys. Chem. Ref. Data* **1990**, *19*, 677−717.
(63) Tao, A. R.; Habas, S.; Yang, P. *Small* **2008**, *4*, 310−325.

DOI: 10.1021/acs.analchem.9b03798
Anal. Chem. 2019, 91, 14639−14648

(64) Kern, A. M.; Martin, O. J. F. *Nano Lett.* **2011**, *11*, 482−487.
(65) Rodríguez-Fernández, J.; Funston, A. M.; Pérez-Juste, J.; Álvarez-Puebla, R. A.; Liz-Marzán, L. M.; Mulvaney, P. *Phys. Chem. Chem. Phys.* **2009**, *11*, 5909.
(66) Perassi, E. M.; Hernandez-Garrido, J. C.; Moreno, M. S.; Encina, E. R.; Coronado, E. A.; Midgley, P. A. *Nano Lett.* **2010**, *10*, 2097−2104.
(67) Hong, S.; Shuford, K. L.; Park, S. *Chem. - Asian J.* **2013**, *8*, 1259−1264.
(68) Pecharromán, C.; Pérez-Juste, J.; Mata-Osoro, G.; Liz-Marzán, L. M.; Mulvaney, P. *Phys. Rev. B: Condens. Matter Mater. Phys.* **2008**, *77*, 035418.
(69) Sun, Y.; Xia, Y. *Science* **2002**, *298*, 2176−2179.
(70) Le Ru, E. C.; Etchegoin, P. G. *SPlaC: SERS and Plasmonics Codes*; School of Chemical and Physical Sciences, Victoria University of Wellington: Wellington, New Zealand, 2009; Matlab codes freely available from http://www.vuw.ac.nz/raman/book/codes.aspx.
(71) Harvey, A. H.; Gallagher, J. S.; Sengers, J. M. H. L. *J. Phys. Chem. Ref. Data* **1998**, *27*, 761−774.
(72) Somerville, W. R. C.; Auguié, B.; Le Ru, E. C. *J. Quant. Spectrosc. Radiat. Transfer* **2016**, *174*, 39−55.
(73) Somerville, W. R. C.; Auguié, B.; Le Ru, E. C. *J. Quant. Spectrosc. Radiat. Transfer* **2012**, *113*, 524−535.
(74) Somerville, W. R. C.; Auguié, B.; Le Ru, E. C. *J. Quant. Spectrosc. Radiat. Transfer* **2013**, *123*, 153−168.

DOI: 10.1021/acs.analchem.9b03798
Anal. Chem. 2019, 91, 14639−14648

Supplementary Information for "Combined extinction and absorption UV–vis spectroscopy reveals shape imperfections of metallic nanoparticles"

Johan Grand, Baptiste Auguié, and Eric C. Le Ru*
The MacDiarmid Institute for Advanced Materials and Nanotechnology, School of Chemical and Physical Sciences, Victoria University of Wellington, PO Box 600, Wellington 6140, New Zealand
(Dated: August 9, 2019)

ADDITIONAL FIGURES

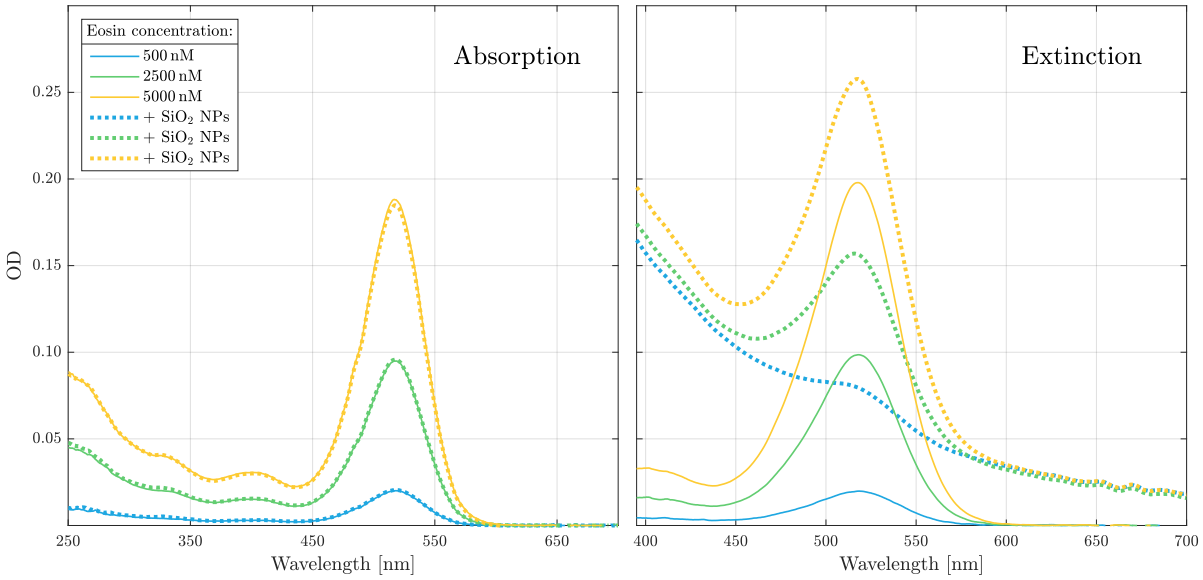

FIG. S1. Absorption (left) and extinction (right) spectra of 3 Eosin B solutions in water (solid lines) recorded simultaneously in the CloudSpec-UV-v0.8. In both graphs, the dotted lines correspond to solutions of Eosin B mixed with a solution of 100 nm amorphous silica NPs coated with carboxylic acid groups. The resulting solution concentrations are the same as for the bare Eosin solutions, namely 500 nM, 2500 nM and 5000 nM. Eosin B and the silica NPs being both negatively charged, the dye molecules are not expected to stick to the NPs. The silica NP concentration was adjusted to match the level of scattering at resonance of the 60 nm silver sphere colloidal solution studied in the article.

* Eric.LeRu@vuw.ac.nz

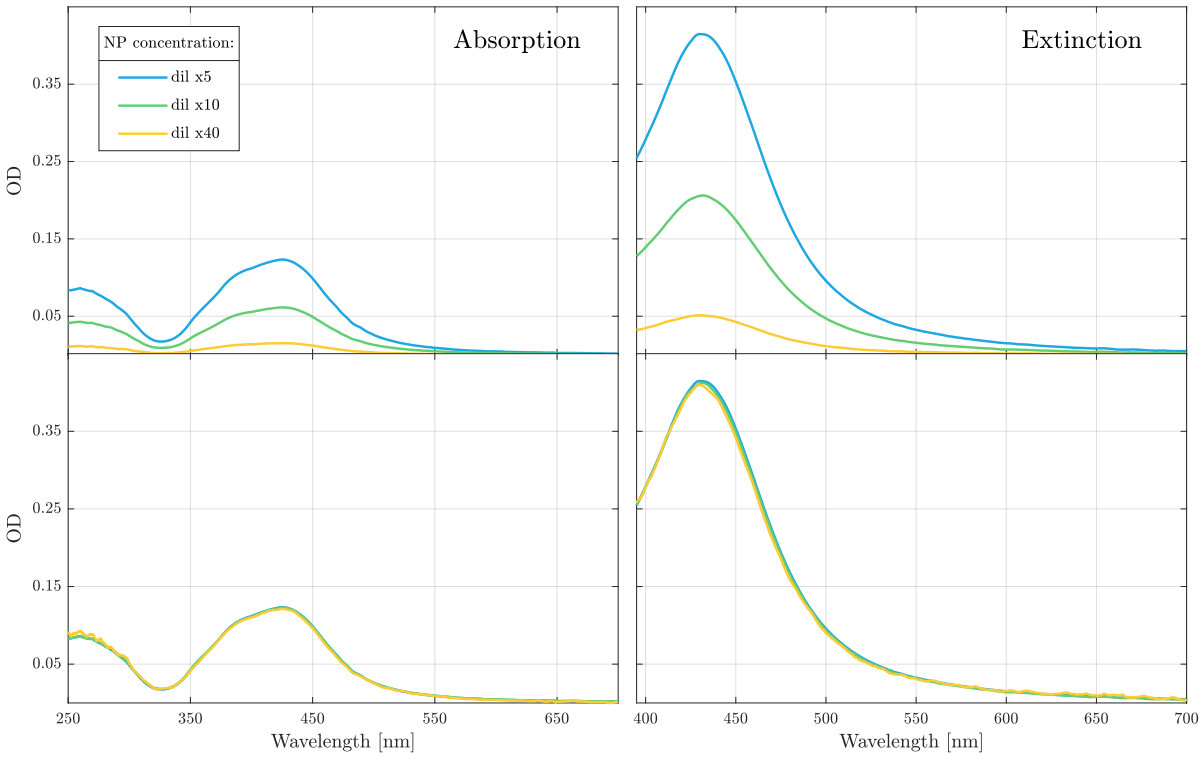

FIG. S2. Absorption (left) and extinction (right) spectra of a 60 nm silver sphere solution recorded with the CloudSpec-UV-v0.8 system. The three curves on each panel represent three different dilution factors ($\times 5$, $\times 10$ and $\times 40$) from the stock solution provided by the NP manufacturer. Bottom plots are corrected by their respective dilution factors.